Inorganic Chemistry

Article

pubs.acs.org/IC

Highly Luminescent Half-Lantern Cyclometalated Platinum(II) Complex: Synthesis, Structure, Luminescence Studies, and Reactivity.

Violeta Sicilia,*[,†] Juan Forniés,[‡] José M[a] Casas,[‡] Antonio Martín,[‡] José A. López,[‡] Carmen Larraz,[‡] Pilar Borja,[‡] Carmen Ovejero,[†] Daniel Tordera,[§] and Henk Bolink[§]

[†]Instituto de Síntesis Química y Catálisis Homogénea (ISQCH), CSIC - Universidad de Zaragoza, Departamento de Química Inorgánica, Escuela de Ingeniería y Arquitectura de Zaragoza, Campus Río Ebro, Edificio Torres Quevedo, 50018, Zaragoza, Spain

[‡]Instituto de Síntesis Química y Catálisis Homogénea (ISQCH), CSIC - Universidad de Zaragoza, Departamento de Química Inorgánica, Facultad de Ciencias, Pedro Cerbuna 12, 50009 Zaragoza, Spain

[§]Universidad de Valencia-Instituto de Ciencia Molecular, Valencia, España

Supporting Information

ABSTRACT: The half-lantern compound $[\{Pt(bzq)(\mu\text{-}C_7H_4NS_2\text{-}\kappa N,S)\}_2]\cdot Me_2CO$ (**1**) was obtained by reaction of equimolar amounts of potassium 2-mercaptobenzothiazolate ($KC_7H_4NS_2$) and $[Pt(bzq)(NCMe)_2]ClO_4$. The Pt(II)···Pt(II) separation in the neutral complex $[\{Pt(bzq)(\mu\text{-}C_7H_4NS_2\text{-}\kappa N,S)\}_2]$ is 2.910 (2) Å, this being among the shortest observed in half-lantern divalent platinum complexes. Within the complex, the benzo[*h*]quinoline (bzq) groups lie in close proximity with most C···C distances being between 3.3 and 3.7 Å, which is indicative of significant $\pi-\pi$ interactions. The reaction of **1** with halogens X_2 (X_2 = Cl_2, Br_2, or I_2) proceeds with a two-electron oxidation to give the corresponding dihalodiplatinum(III) complexes $[\{Pt(bzq)(\mu\text{-}C_7H_4NS_2\text{-}\kappa N,S)X\}_2]$ (X = Cl **2**, Br **3**, I **4**). Their X-ray structures confirm the retention of the half-lantern structure and the coordination mode of the bzq and the bridging ligand $\mu\text{-}C_7H_4NS_2\text{-}\kappa N,S$. The Pt–Pt distances (Pt–Pt = 2.6420(3) Å **2**, 2.6435(4) Å **3**, 2.6690(3) Å **4**) are shorter than that in **1** because of the Pt–Pt bond formation. Time dependent-density functional theory (TD-DFT) studies performed on **1** show a formal bond order of 0 between the metal atoms, with the $6p_z$ contribution diminishing the antibonding character of the highest occupied molecular orbital (HOMO) and being responsible for an attractive intermetallic interaction. A shortening of the Pt–Pt distance from 2.959 Å in the ground state S_0 to 2.760 Å in the optimized first excited state (T_1) is consistent with an increase in the Pt–Pt bond order to 0.5. In agreement with TD-DFT calculations, the intense, structureless, red emission of **1** in the solid state and in solution can be mainly attributed to triplet metal–metal-to-ligand charge transfer (^{3}MMLCT) [$d\sigma^*(Pt–Pt) \rightarrow \pi^*(bzq)$] excited states. The high quantum yields of this emission measured in toluene (44%) and solid state (62%) at room temperature indicate that **1** is a very efficient and stable ^{3}MMLCT emitter, even in solution. The high luminescence quantum yield of its red emission, added to its neutral character and the thermal stability of **1**, make it a potential compound to be incorporated as phosphorescent dopant in multilayer organic light-emitting devices (OLEDs).

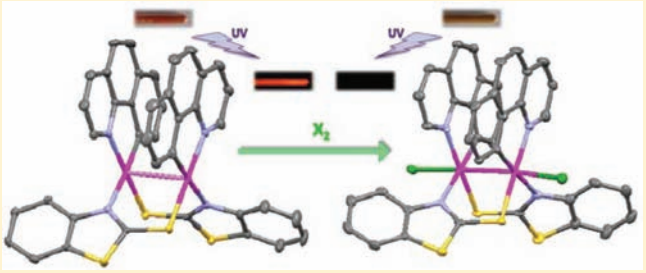

INTRODUCTION

Recently much attention has been paid to luminescent cyclometalated Pt(II) complexes due to their attractive photochemical and photophysical properties, and they have been the subject of some excellent, comprehensive reviews.[1−5] Many of these complexes have been successfully applied as phosphorescent dopants in the manufacture of highly efficient organic light-emitting devices (OLEDs).[3,4,6−8]

In these kinds of compounds, monomer emission typically arises from triplet ligand-centered (^{3}IL), metal-to-ligand charge transfer (^{3}MLCT) and metal–ligand-to-ligand charge transfer (^{3}MLL′CT) excited states.

In addition, monomer square-planar Pt(II) neutral complexes with sterically undemanding ligands have long been known to have a great tendency to self-assemble, in the axial direction, into linear chains, dimers, or Pt_3 structures directed by Pt···Pt interactions.[9−17] When nonbulky π-extended ligands such as diimines, terpyridines, or C,N-cyclometalated ligands are present, then $\pi\cdots\pi$ interactions, in addition to Pt···Pt, play a significant structure-directing role.[18−20] Stacked linear compounds or oligomers with such Pt···Pt and/or $\pi\cdots\pi$ interactions display phosphorescence derived from metal–metal-to-ligand charge transfer (^{3}MMLCT) and/or $^3\pi-\pi^*$ excimeric excited states.[1,21−30] In general, absorptions and emissions in such systems are strongly dependent on the extent of Pt···Pt and/or $\pi\cdots\pi$ interactions and consequently are influenced by crystallization conditions, solvent, concentration, temperature, and the

Received: September 1, 2011
Published: February 24, 2012

   dx.doi.org/10.1021/ic201910t | *Inorg. Chem.* 2012, 51, 3427−3435

nature of the counterion.[20,24,30−32] The photophysical properties associated with Pt···Pt and $\pi\cdots\pi$ interactions most often disappear in a diluted solution of the complexes as these interactions become weaker or nonexistent.[16,33] This is the reason why the use of auxiliary ligands, able to act as four-bond bridging groups to build rigid metal frameworks with short metal−metal distances even in solution, is an appropriate strategy for obtaining stable ^{3}MMLCT emitters.[34,35]

Discrete dinuclear Pt(II) complexes with a well-defined Pt−Pt distance, using pop (*P*,*P*-pyrophosphite, $P_2O_5H_2^{2-}$),[36,37] PPi (pyrophosphate, $P_2O_7^{4-}$),[38] pyt (pyridine-2-thiolate),[35,39−41] amidate,[42,43] or dppm (diphenylphosphinomethane)[44] as bridging ligands, have long been known. More recently, the dinuclear *anti*- and *syn*-$[\{Pt(d\text{-}t\text{-}bpy)(NS_2)\}_2]$ (d-t-bpy = 4,4′-di*tert*-butyl-2,2′-bipyridine, NS_2 = 2-mercaptobenzothiazolate, 2-mercaptobenzimidazolate, 2-mercaptobenzoxazolate)[45] complexes have been reported. A simplified molecular orbital approach considers that the axial interactions of the metal centers cause the valence d_z^2 orbitals to overlap to give bonding ($d\sigma$) and antibonding ($d\sigma^*$) orbitals;[46] the antibonding character of the highest occupied molecular orbital (HOMO) of dinuclear d^8-d^8 complexes may explain why oxidation leads to enhanced metal−metal bonding on going from diplatinum(II) to diplatinum(III) complexes.[34−36,39,47] Most platinum(III) dimers reported up until now have been prepared either by reaction of the Pt(II) complex with the bridging ligand at high temperature under atmospheric oxygen or by oxidation of the precursor binuclear platinum(II) complexes.[34,35,48,49] However, not many structures of related Pt_2(III−III) compounds can be found in the literature to compare the influence of axial ligands on the Pt(III)−Pt(III) distance.[36,47] The d^7-d^7 complexes are in general nonemissive either in solution or in the solid state with just a few exceptions as $[Pt_2(\mu\text{-}pop)_4X_2]^{4-}$ (pop = *P*,*P*-pyrophosphite, $P_2O_5H_2^{2-}$, X = Cl, Br, SCN, or py)[46,50] that exhibit red luminescence in an alcohol glass or in solid state at low temperature and $[\{Pt(\kappa^2\text{-}As,C\text{-}C_6H_3\text{-}5\text{-}CHMe_2\text{-}2\text{-}AsPh_2)_2X\}_2]$ (X = Cl, Br, I, CN)[34] that emit in the visible to near infrared (NIR) region even at room temperature.

In the course of our research on luminescent Pt(II) complexes, with the aim of obtaining stable ^{3}MMLCT emitters, we prepared a new half-lantern Pt(II) complex $[\{Pt(bzq)(\mu\text{-}C_7H_4NS_2\text{-}\kappa N,S)\}_2]$ containing benzo[*h*]quinoline (bzq) as the cyclometalated ligand and 2-mercaptobenzothiazolate as the bridging group. The high quantum yield of its emission, its neutral character, and thermal stability make it a good material for application in the manufacturing of OLEDs. The interesting luminescence properties of this complex have also been studied by time-dependent-density functional theory (TD-DFT) calculations. Furthermore, the two-electron-oxidized dinuclear Pt(III) complexes $[\{Pt(bzq)(\mu\text{-}C_7H_4NS_2\text{-}\kappa N,S)X\}_2]$ (X = Cl, Br, I) have been prepared and their X-ray structures compared.

RESULTS AND DISCUSSION

Synthesis and Characterization of $[\{Pt(bzq)(\mu\text{-}C_7H_4NS_2\text{-}\kappa N,S)\}_2]\cdot Me_2CO$ (1) and $[\{Pt(bzq)(\mu\text{-}C_7H_4NS_2\text{-}\kappa N,S)X\}_2]$ [X = Cl (2), Br (3), I (4)]. $[\{Pt(bzq)(\mu\text{-}C_7H_4NS_2\text{-}\kappa N,S)\}_2]\cdot Me_2CO$ (**1**) was obtained by reaction of equimolar amounts of $KC_7H_4NS_2$ and $[Pt(bzq)(NCMe)_2]ClO_4$ in acetone/methanol (2:1). Compound **1** precipitated in the reaction mixture from which it was separated and recrystallized as a pure orange-red solid. The presence of acetone in the powdered samples of **1** is evident in its IR spectrum ($\upsilon_{C=O}$, 1704 cm^{-1}), ^{1}H NMR spectrum (2.12 ppm, 6H), and elemental analysis (see the Experimental Section). The ^{1}H NMR and ^{195}Pt NMR spectra show the set of signals corresponding to the half of the molecule indicating that compound **1** was isolated as one single and symmetric isomer (the anti one). The X-ray molecular structure of the dinuclear complex $[\{Pt(bzq)(\mu\text{-}C_7H_4NS_2\text{-}\kappa N,S)\}_2]$ is shown in Figure 1, and selected bond distances and angles are listed in Table 1. As can be seen, complex $[\{Pt(bzq)(\mu\text{-}C_7H_4NS_2\text{-}\kappa N,S)\}_2]$ is a neutral dinuclear species of Pt(II) formed by two fragments "Pt(bzq)" doubly bridged by two 2-mercaptobenzothiazolate ($\mu\text{-}C_7H_4NS_2\text{-}\kappa N,S$) groups in

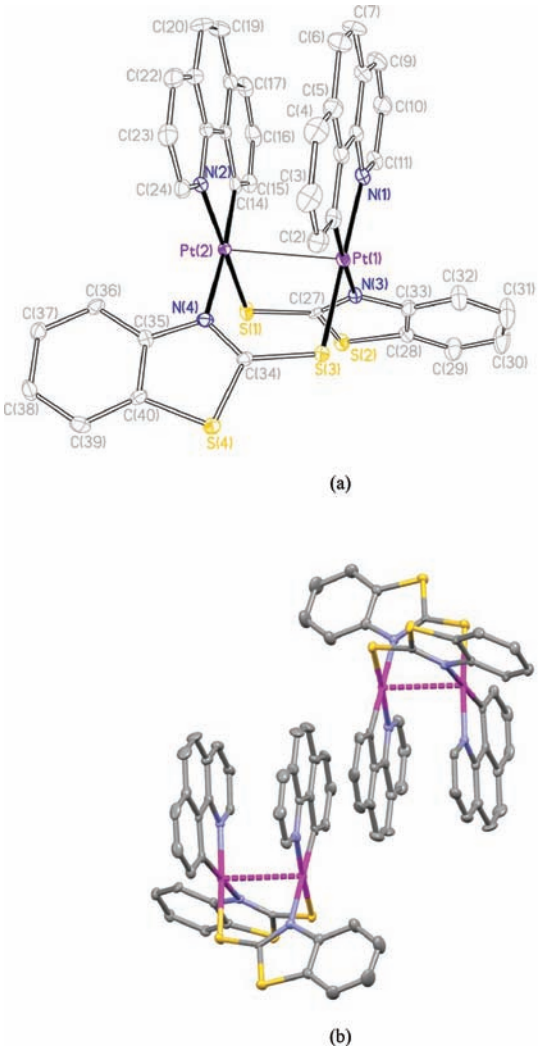

Figure 1. Molecular structure of the dinuclear complex in **1**. Ellipsoids are drawn at their 50% probability level; solvent molecules and hydrogen atoms were omitted for clarity (a); X-ray packing view showing intra- and intermolecular $\pi-\pi$ interactions (b).

Table 1. Selected Bond Distances (Å) and Angles (deg) of 1

Pt1−C1: 1.993(3)	Pt2−S1: 2.287(8)
Pt1−N1: 2.060(2)	Pt2−C14: 1.997(3)
Pt1−N3: 2.135(2)	Pt2−N2: 2.047(2)
Pt1−S3: 2.285(2)	Pt2−N4: 2.129(2)
Pt1−Pt2: 2.9101(18)	
C(1)−Pt(1)−N(1): 81.66(11)	C(14)−Pt(2)−N(2): 82.57(11)
N(1)−Pt−N(3): 95.63(10)	N(2)−Pt(2)−N(4): 93.59(9)
C(1)−Pt(1)−S(3): 94.78(9)	C(14)−Pt(2)−S(1): 93.61(9)
N(3)−Pt(1)−S(3): 87.90(7)	N(4)−Pt(2)−S(1): 90.11(7)

dx.doi.org/10.1021/ic201910t | *Inorg. Chem.* 2012, 51, 3427−3435

such a way that the molecule shows an anti configuration and an intermetallic separation of 2.910(2) Å. The Pt(II)···Pt(II) separation is similar to that found in the *syn*-$[Pt_2(bpy)_2(pyt)_2]$[40] and $[Pt_2(dtbpy)_2(pyt)_2]$[41] complexes and is among the shortest observed in half-lantern divalent platinum complexes.[35,38,40−43,45] This distance is longer than that found in some full-lantern divalent platinum complexes, such as $[Pt_2(4\text{-mpyt})_4]$(2.680(2) Å),[39] or $[Pt_2(CH_3CSS)_4]$(2.767(1) Å),[51] but it is shorter than that observed in neutral 1D stacked square-planar Pt(II) complexes (Pt···Pt, 3.09−3.50 Å).[10,12−17,32,52] Each Pt(II) center coordinates to the two donor atoms of the benzoquinolinate ligand (C, N) a N atom of one 2-mercapto-benzothiazolate (NS_2), and an S atom of the other one. Each Pt(II) center shows a distorted square-planar environment with the distortion mainly being due to the small bite angle of the C,N-cyclometalated ligand [81.7(1)° Pt(1), 82.6(1)° Pt(2)]. This anti isomer has a head-to-tail configuration of the two bridging NS_2 groups with a 2-fold axis perpendicular to the midpoint of the Pt(II)···Pt(II) line. Bond distances and angles are similar to those observed in other Pt(II) complexes containing bzq[16,30,53,54] or N^S bridging ligands such as pyridin-2-thiolate,[35,39−41] or 2-mercaptobenzothiazolate.[45] The longer $Pt-N_{\hat{N}S}$ (2.135(2) Å Pt(1), 2.129(2) Å Pt(2)) distances related to $Pt-N_{bzq}$ ones (2.060(2) Å Pt(1), 2.047(2) Å, Pt(2)) agree with the larger trans influence of C with respect to S. The platinum coordination planes are not completely parallel to one another since the interplanar angle is 11.3(1)°. Regarding the bzq groups, an anti arrangement of identical donor atoms is found. Inside the complex, the two bzq are nearly parallel but not eclipsed (torsion angle N(1)−Pt(1)−Pt(2)−N(2), 64.4(1)°) presumably to minimize repulsions, as is usual in C,N-cyclometalated compounds. The bzq groups are close to one another with most C−C distances between 3.3 and 3.7 Å, which are indicative of significant $\pi-\pi$ interactions.[16,17,35]

The short Pt···Pt distance (less than 3.5 Å) and the perpendicularity between the Pt−Pt line and both metal coordination planes (angles = 6.9(1)°, Pt(1); 8.0(1)°, Pt(2)) suggest a significant interaction of the $5d_{z^2}$ orbitals of both platinum centers. Within the crystal, weak intermolecular $\pi\cdots\pi$ interactions give rise to the packing of the molecules by dimers (Figure 1b) with many C−C distances between 3.65 and 3.78 Å.

As expected from the short Pt−Pt distance, compound **1** undergoes two-electron oxidation upon treatment with halogens X_2 (X_2 = Cl_2, Br_2, or I_2) to give the corresponding dihalodiplatinum(III) complexes $[\{Pt(bzq)(\mu\text{-}C_7H_4NS_2\text{-}\kappa N,S)X\}_2]$ (X = Cl **2**, Br **3**, I **4**) as yellow-brown, brown, and purple solids, respectively. Small and similar changes in the IR and ^1H NMR spectra of powdered samples of **2**−**4** with respect to the starting complex, **1**, indicate that the resulting Pt(III) complexes are similar to each other, as was confirmed by X-ray crystallography. The X-ray structures of **2**, **3**, and **4** can be seen in Figure 2a and in Figures S1a and S2a in the Supporting Information, respectively, and a selection of bond distances and angles in Table 2. They confirm the retention of the half-lantern structure and the coordination mode of the bzq and the bridging ligand $\mu\text{-}C_7H_4NS_2\text{-}\kappa N$, S with respect to the starting complex **1**. Each Pt(III) center has a distorted octahedral environment with the axial positions occupied by an halogen atom (Cl **2**, Br **3**, I **4**) and the other Pt(III) center and with the X−Pt−Pt angles being close to 173°. Compounds **2**−**4** show shorter Pt−Pt distances than **1** because of the Pt−Pt bond existence (Pt−Pt = 2.6420(3) Å **2**, 2.6435(4) Å **3**, 2.6690(3) Å **4**). These distances are in the range of those observed in Pt_2(III, III) complexes.[34−36,39,47] The trend of increasing Pt−Pt distances is in accordance with the trans-influence of the axial ligand (Cl < Br < I),[55] as was previously observed in $[Pt_2(P_2O_5H_2)_4X_2]^{4-}$ (X = Cl, Br, I),[47] $[Pt_2(\mu\text{-}\kappa As,\kappa C\text{-}C_6H_3\text{-}5\text{-}CHMe_2\text{-}2\text{-}AsPh_2)_4X_2]$ (X = Cl, Br, I)[34] or $[Pt_2(\mu\text{-}\kappa As,\kappa C\text{-}C_6H_3\text{-}5\text{-}Me\text{-}2\text{-}AsPh_2)_4X_2]$ (X = Cl, Br, I).[56]

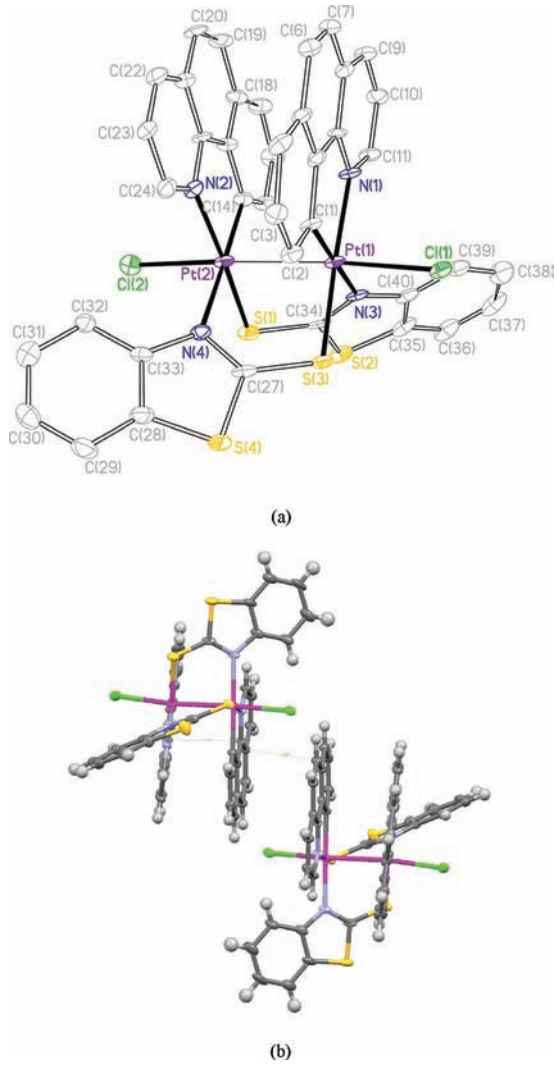

Figure 2. Molecular and supramolecular structures of compound **2**. Ellipsoids are drawn at their 50% probability level; solvent molecules and hydrogen atoms were omitted for clarity (a). X-ray packing view showing intra- and intermolecular $\pi-\pi$ interactions (b).

The Pt(III)−X distances are in the range of those found in other complexes with this kind of ligand. In the dinuclear Pt_2(III,III) complexes **2**−**4**, the two platinum coordination planes are almost parallel, and the interplanar angle [4.2(1)° (**2**), 5.7(1)° (**3**) and 6.1(1)° (**4**)] is smaller than in the Pt_2(II,II) complex **1**. Perpendicularity between the Pt−Pt line and both of the Pt square coordination planes is higher than in complex **1**, the biggest angle being 3.6(1)° (linear Pt1−Pt2 and Pt1 plane for compound **4**).

The crystal packing of the dichloro complex, **2**, is almost equal to that observed in the starting Pt(II) complex (Figure 2b); however, the crystal packing of complexes **3** and **4** are similar but different from **1** and **2** with no $\pi\cdots\pi$ bzq intermolecular interactions, as can be seen in Figures S1b and S2b in the Supporting Information.

Photophysical and Computational Studies. *Absorption Spectra.* Electronic absorption spectra of **1** were recorded

dx.doi.org/10.1021/ic201910t | *Inorg. Chem.* 2012, 51, 3427−3435

Table 2. Selected Bond Distances (Å) and Angles (deg) of 2, 3, and 4

	2·2.5CH_2Cl_2	**3**·3CH_2Cl_2	**4**·3CH_2Cl_2
Pt(1)−C(1)	2.017(5)	2.026(6)	2.026(6)
Pt(1)−N(1)	2.087(4)	2.064(5)	2.078(5)
Pt(1)−N(3)	2.228(5)	2.198(5)	2.198(5)
Pt(1)−S(3)	2.3007(13)	2.3007(16)	2.3014(14)
Pt(1)−X(1)	2.4609(14)	2.5569(7)	2.7601(4)
Pt(1)−Pt(2)	2.6420(3)	2.6435(4)	2.6690(3)
Pt(2)−C(14)	2.031(5)	2.020(6)	2.017(6)
Pt(2)−N(2)	2.082(5)	2.065(5)	2.063(5)
Pt(2)−N(4)	2.198(4)	2.184(5)	2.192(5)
Pt(2)−S(1)	2.2986(14)	2.2884(15)	2.3031(14)
Pt(2)−X(2)	2.4512(15)	2.5985(7)	2.7518(4)
C(1)−Pt(1)−N(1)	81.84(19)	82.5(2)	81.9(2)
N(1)−Pt(1)−N(3)	96.15(17)	94.2(2)	95.6(2)
C(1)−Pt(1)−S(3)	94.35(15)	95.6(2)	94.65(18)
N(3)−Pt(1)−S(3)	87.73(12)	87.80(14)	87.88(13)
C(14)−Pt(2)−N(2)	82.4(2)	82.5(3)	81.9(2)
N(2)−Pt(2)−N(4)	95.78(17)	94.8(2)	94.13(19)
C(14)−Pt(2)−S(1)	94.27(16)	94.8(2)	95.82(18)
N(4)−Pt(2)−S(1)	87.53(12)	87.95(14)	88.21(13)
C(1)−Pt(1)−X(1)	86.46(16)	84.2(2)	84.03(17)
N(1)−Pt(1)−X(1)	89.51(13)	90.43(17)	90.97(14)
N(3)−Pt(1)−X(1)	94.65(13)	96.27(14)	96.90(13)
S(3)−Pt(1)−X(1)	86.41(5)	86.06(4)	85.39(4)
Pt(2)−Pt(1)−X(1)	174.17(3)	172.416(18)	171.681(13)
C(14)−Pt(2)−X(2)	86.38(16)	84.82(19)	83.14(18)
N(2)−Pt(2)−X(2)	89.20(13)	91.40(18)	90.72(13)
N(4)−Pt(2)−X(2)	93.83(13)	95.75(15)	97.87(13)
S(1)−Pt(2)−X(2)	85.66(5)	84.55(4)	86.04(4)
Pt(1)−Pt(2)−X(2)	173.86(4)	171.515(18)	171.620(13)

Table 3. Photophysical Data of 1

absorption 298 K	λ_{abs}/nm (10^3 ε M^{-1} cm^{-1})		
solid	326, 420sh, 500		
2-Me-THF 10^{-4} M	296(32.9), 308(32.9), 322(29.2), 334(24.9), 342sh(23.8), 350sh(21.0), 389(9.3), 426(4.7), 496(2.9)		
CH_2Cl_2 10^{-4} M	298(34.1), 308(34.7), 322(30.7), 334(25.6), 342sh(24.6), 350sh(22.1), 388(9.4), 426(4.7), 487(2.9)		
toluene 10^{-4} M	288(29.7), 300(32.7), 310(34.7), 322(32.4), 334(26.4), 342sh(25.7), 350sh(23.4), 394(10.7), 427(5.4), 500(3.1)		
DMF 10^{-4} M	300 (30.0), 310 (30.9), 322 (28.1), 334 (24.0), 342sh (22.9), 350sh (20.2), 383 (8.4), 416 (4.7), 482 (2.6)		
emission	λ_{exc}(nm)	λ_{em}(nm) [Φ]	τ (μs)
solid 77 K	520	643	2.3
solid 298 K	550	665	1.9
PL in film 5 wt % complex in PMMA	386	628 [0.62]	
CH_2Cl_2 10^{-3} M 77 K	530	679	2.5
CH_2Cl_2 10^{-3} M 298 K	530	679	0.1
CH_2Cl_2 10^{-6} M 298 K	340	665 [0.19]	
toluene 10^{-5} M 298 K	338	677 [0.44]	
2-Me-THF 10^{-3}M 77 K	445−480	600_{sh}, 650_{sh},691_{max} tail to 780	
	530	625_{sh}, 650_{sh},692_{max} tail to 780	5.8 (692)
2-Me-THF 10^{-3} M 298 K	400−520	681	0.7
2-Me-THF 10^{-4}M 77 K	430	492, 527, 652_{max}, 679 tail to 780	29.4 (71%), 147.6 (29%) (492); 5.3 (650)
	520	650_{max}, 670 tail to 780	
2-Me-THF 10^{-4} M 298 K	400−520	684	

in several solvents with increasing polarity (toluene, 2-Me-THF, CH_2Cl_2, and DMF), and the data obtained are summarized in Table 3. The spectra are shown in Figure 3. They reveal intense absorptions (ε > 20 000 M^{-1} cm^{-1}) at λ < 350 nm, attributable to $\pi-\pi^*$ intraligand (IL, bzq, NS_2) transitions (Figure S3 in the Supporting Information) and some weaker absorptions at λ values ranging from 350 to 450 nm, which are likely due to admixtures of metal-perturbed intraligand transitions (^{1}IL), ligand-to-ligand charge transfer (LLCT), and metal-to ligand charge transfer (^{1}MLCT) transitions.[16,30,57] In addition, they show a less intense, low-energy feature, maximizing at ∼490−500 nm, which could be assigned to metal−metal-to ligand charge transfer (^{1}MMLCT) [dσ^*(Pt−Pt) → π^*(bzq)] transitions, which arose from the Pt···Pt interactions likely to

dx.doi.org/10.1021/ic201910t | Inorg. Chem. 2012, 51, 3427−3435

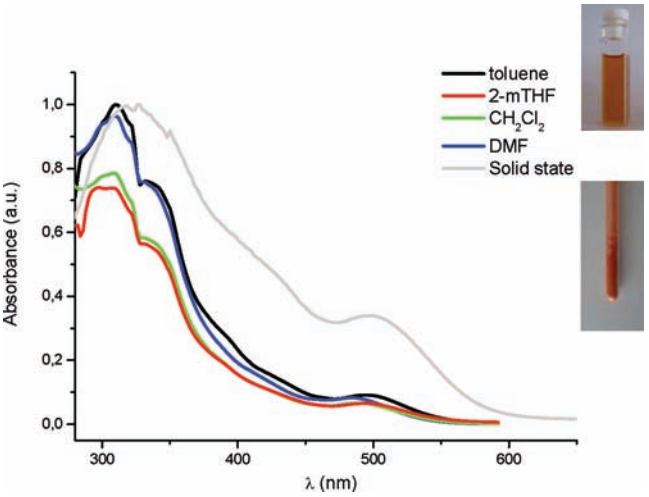

Figure 3. Normalized absorption spectra in different solvents (10^{-4} M) and normalized diffuse reflectance UV–vis (DRUV) spectrum of **1** in the solid state at room temperature. Side pictures: **1** in CH_2Cl_2 solution and the solid state.

have been affected by the $\pi\cdots\pi$ contacts in this diplatinum (II,II) complex, **1** as in other dinuclear pyridinethiolate Pt(II) complexes $[Pt_2L_2(pyt)_2]$.[35] In addition, our DFT calculations (see Figure 4 and Tables S1 and S2 in the Supporting Information) indicate the lowest unoccupied molecular orbital (LUMO) is located on the bzq ligand and the HOMO to be mainly a d_{z^2} σ^* Pt–Pt antibonding orbital, the H-1 orbital to be composed of d(Pt) (27%)/p(S) (43%)/NS_2–S (26%) and the HOMO → LUMO, HOMO → L + 1, and H − 1 → LUMO to be the main transitions involved in the S1, S2, and S3 calculated excitation. It is for this reason that the lower energy absorption band of **1** in solution could be mainly due to ^{1}MMLCT transitions with some ^{1}MLLCT character. This lower absorption band shows a modest negative solvatochromism from toluene to DMF (see Table 3 and Figure 3) and follows Beer's law in the concentration range from 2×10^{-5} to 5×10^{-3} M (Figure S4 in the Supporting Information), indicating that aggregations of dimers do not occur within this range. The similarity of the diffuse reflectance UV–vis spectrum (DRUV) of a solid sample of **1** with its UV–vis spectra in solution indicates nonsignificant structural changes or molecular aggregation upon crystallization. Hence, analogous assignment of the absorption bands can be performed.

Emission Spectra. Complex **1** exhibits red luminescence not only in the solid state but also in solution at room temperature. Table 3 summarizes all the emission data. The emission spectra of **1** in CH_2Cl_2 (10^{-4} M) and 2-Me-THF (10^{-4} M) (Figure 5 and Figure S5 in the Supporting Information, respectively) show quite similar, structureless profiles both in solution at 298 K and in the rigid matrix at 77 K upon excitation at a λ of ∼525 nm. DFT calculations on **1** show a good agreement among the experimental excitation spectrum in CH_2Cl_2 monitored at λ_{em} = 680 nm and the lower energy excitation states (see Figure 4 and Tables S1 and S2 in the Supporting Information), which allows this emission to be attributed to ^{3}MMLCT $[d\sigma^*(Pt)_2 \rightarrow \pi^*(bzq)]$ excited states. Excitation at 550 nm of powdered orange-red samples of **1** at room temperature leads to an intense structureless emission band, with its maximum at λ_{max} = 665 nm (Figure 6) that becomes narrower and slightly blue-shifted upon cooling to 77 K. We attribute this significant decrease in the bandwidth at 77 K to a smaller distortion of

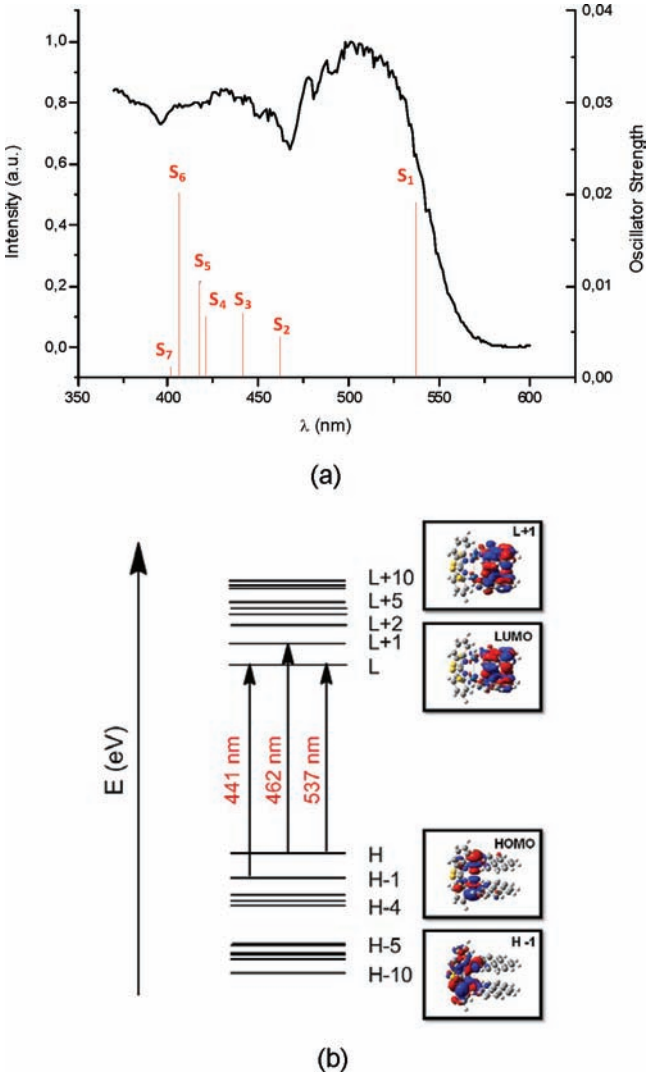

Figure 4. (a) Experimental excitation spectra of compound **1** in CH_2Cl_2(10^{-4} M) at 77 K (black) and calculated transitions in CH_2Cl_2 solution (red bars); (b) most important transitions (>95%) involved in lower energy excited calculated states (S1, S2, S3).

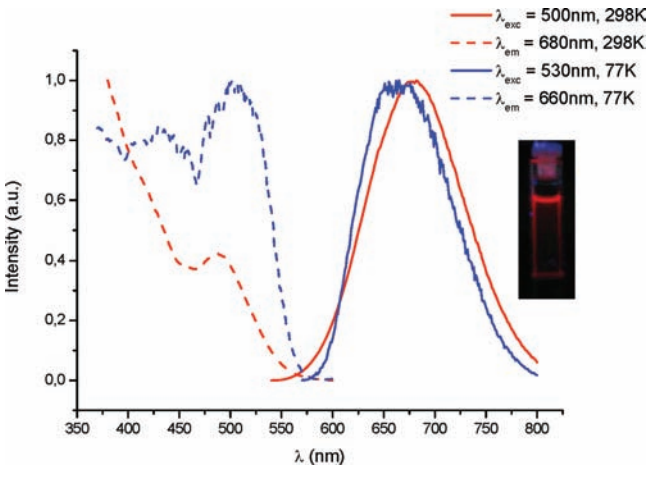

Figure 5. Normalized excitation and emission spectra of **1** in CH_2Cl_2(10^{-4} M) at different temperatures.

the excited state geometry with respect to the ground state at this temperature (Franck–Condon principle). Luminescence

dx.doi.org/10.1021/ic201910t | Inorg. Chem. 2012, 51, 3427–3435

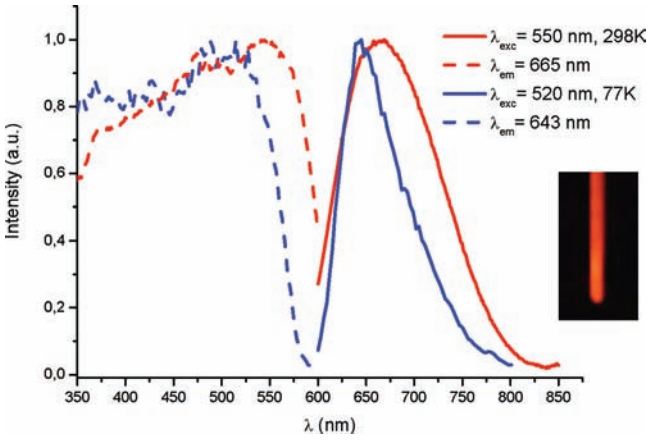

Figure 6. Normalized excitation and emission spectra of **1** in the solid state at 298 and 77 K.

features as band shape, energy, lifetime, and small changes observed upon cooling to 77 K are similar to those observed in other stable diplatinum (II, II) systems with short Pt···Pt contacts.[29,34,35] Quantum yield determinations indicate that **1** is a very good emitter at room temperature in solution and an even better one in the solid state with quantum yields of 44% in toluene solution and 62% in the solid state. When **1** is compared with the closely related compounds, $[\{Pt(bzq)(pyt)\}_2]$ that is also a benzoquinolinate Pt(II) complex, with pyridinethiolate as a four-bond bridging ligand, and $[Pt(d\text{-}t\text{-}bpy)(NS_2)]_2(ClO_4)_2$, which is a diimine complex containing 2-mercaptobenzothiazolate (μ-$C_7H_4NS_2$-κN,S) as four-bond bridging ligand, some differences can be found. The quantum yields of the emission of **1**, both in solution and in the solid state, are considerably higher than those measured for the analogous ^{3}MMLCT emitter $[\{Pt(bzq)(pyt)\}_2]$, which reach up to 14% in the solid state and there is almost no emission in solution at room temperature.[35] In the case of $[Pt(d\text{-}t\text{-}bpy)(NS_2)]_2(ClO_4)_2$,[45] a green emission from MLLCT excited states instead of a red one from ^{3}MMLCT is observed. Thus, **1** formed from "Pt(bzq)" and (μ-$C_7H_4NS_2$-κN,S) as four-bond bridging ligand has turned out to be a very efficient, stable ^{3}MMLCT emitter, both in the solid state and in solution. In addition, the thermo-gravimetric analysis (TGA) of **1**-[**OCMe$_2$**] indicates that it is stable under argon at 1 atm to 350 °C (Figure S6 in the Supporting Information) and then presumably stable enough toward sublimation under vacuum and suitable for the vapor deposition process required for producing OLEDs. The neutral character of **1**, its thermal stability, and its quantum efficiency make it a potential compound to be incorporated in multilayer OLEDs.[5,58,59]

The dimeric Pt(III) complexes **2**–**4** were nonemissive in the visible region (up to 850 nm), as was expected in view of the common behavior of d^7–d^7 complexes.[34]

Density Functional Theory Analysis. TD-DFT studies performed on **1** provided a calculated structure (intermetallic distance of 2.959 Å and a N_{bzq}–Pt–Pt–N_{bzq} torsion angle of 60.2°, see Figure S7 and Table S3 in the Supporting Information) that shows a good agreement with the experimental one. Selected MOs of **1** involved in the main excited states have been drawn in Figure S8 in the Supporting Information, and their relative compositions in terms of component fragments are listed in Table S2 in the Supporting Information. Calculations on **1** show that the HOMO is mainly a d_{z^2} σ* Pt–Pt antibonding orbital (76%) with a small contribution from the $6p_z$ orbital (2%) and orbitals of the ligands (12% bzq, 9% NS_2) while the LUMO, L + 1, L + 2 are located on the bzq ligand and are mainly ligand in character. Despite the formal bond order of 0 between the metal atoms, the $6p_z$ contribution diminishes the antibonding character of the HOMO (see Figure S8 in the Supporting Information) and is responsible for an attractive intermetallic interaction.[60] The first excited state (T_1) was also optimized, and it shows a very similar structure (Table S4 in the Supporting Information) but without symmetry and with a shortening of the Pt–Pt distance from 2.959 Å in the ground state S_0 to 2.760 Å in the excited state T_1, consistent with an increase in the Pt–Pt bond order to 0.5. Furthermore, the theoretical values for the $S_0 \rightarrow S_1$ transition (~537 nm) compare well with the lowest experimental excitation band, as can be seen in Figures 4 and 6; its major contribution involves the HOMO → LUMO (98%) transition, which indicates its MMLCT character. The same character is attributable to the $S_0 \rightarrow S_2$ transition (~462 nm) with a major contribution from the HOMO → L + 1 (98%) transition. Other calculated absorptions above 400 nm agree well with experimental data and show a remarkable MMLCT character in most of them. These calculations confirm that the emission of **1** at ~650 nm, both in solution and in the solid state, takes place from MMLCT excited states.

CONCLUSIONS

The half-lantern compound $[\{Pt(bzq)(\mu\text{-}C_7H_4NS_2\text{-}\kappa N,S)\}_2]\cdot Me_2CO$ (**1**) was obtained by reaction of equimolar amounts of $KC_7H_4NS_2$ and $[Pt(bzq)(NCMe)_2]ClO_4$. The Pt(II)···Pt(II) separation in the neutral complex $[\{Pt(bzq)(\mu\text{-}C_7H_4NS_2\text{-}\kappa N,S)\}_2]$ is 2.910(2) Å, this being among the shortest observed in half-lantern divalent platinum complexes. Compound **1** undergoes two-electron oxidation upon the treatment with halogens X_2 (X_2 = Cl_2, Br_2, or I_2) to give the corresponding diplatinum(III) complexes $[\{Pt(bzq)(\mu\text{-}C_7H_4NS_2\text{-}\kappa N,S)X\}_2]$ (X = Cl **2**, Br **3**, I **4**). Their X-ray structures confirm the retention of the half-lantern structure and the shortening of the Pt–Pt distances (Pt–Pt = 2.6420(3) Å **2**, 2.6435(4) Å **3**, 2.6690(3) Å **4**) with respect to **1** because of the Pt–Pt bond formation.

TD-DFT studies performed on **1** show a formal bond order of 0 between the metal atoms, with the $6p_z$ contribution being responsible for an attractive intermetallic interaction. A shortening of the Pt–Pt distance from 2.959 Å in the ground state S_0 to 2.760 Å in the optimized first excited state (T_1) is consistent with an increase in the Pt–Pt bond order to 0.5. The lower energy absorption band of **1** at room temperature (λ_{max} ~490 nm) seems to be mainly due to ^{1}MMLCT transitions with some ^{1}MLLCT character and the intense, structureless red emission mainly attributed to ^{3}MMLCT [$d\sigma^*(Pt)_2 \rightarrow \pi^*(bzq)$] excited states, on the basis of the TD-DFT calculations. The high quantum yields of the emissions measured in toluene and solid state at room temperature indicate that **1** is a very efficient and stable ^{3}MMLCT emitter, even in solution. The neutral character of **1**, its thermal stability, the short lifetime, and high luminescence quantum yield of its red emission make it a potential compound to be incorporated in multilayer OLEDs.

Similar works using 2-mercaptobenzoxazolate (NOS^-), 2-mercaptopyrimidinate (N_2S^-), and 2-mercapto-1-methylimidazolate (Me-N_2S^-) as bridging groups are in progress.

dx.doi.org/10.1021/ic201910t | Inorg. Chem. 2012, 51, 3427–3435

EXPERIMENTAL SECTION

General Procedures and Materials. Elemental analyses were carried out with a Perkin-Elmer 2400 CHNS analyzer. IR spectra were recorded on a Perkin-Elmer Spectrum 100 FT-IR spectrometer (ATR in the range 250−4000 cm^{-1}). Mass spectrometry was performed with the Microflex matrix-assisted laser desorption ionization-time-of-flight (MALDI-TOF) Bruker or an Autoflex III MALDI-TOF Bruker instruments. Thermogravimetric analysis (TGA) was performed in the range 20−600 at 10 °C/min under nitrogen atmosphere using a STD 2960 simultaneous DTA-TGA from TA Instruments. NMR spectra were recorded on a Bruker ARX-300 or Bruker AV-400 spectrometer using the standard references: $SiMe_4$ for ^1H and Na_2PtCl_6 in D_2O for ^{195}Pt. The ^{195}Pt spectrum was proton-decoupled, J is given in Hz, and assignments are based on $^1H-^1H$ correlation spectroscopy (COSY) experiments. Diffuse reflectance UV−vis (DRUV) spectra were recorded on a Thermo Electron Corporation evolution 600 spectrophotometer equipped with a Praying Mantis integrating sphere. The solid samples were homogeneously diluted with silica. The mixtures were placed in a homemade cell equipped with a quartz window. Steady-state photoluminescence spectra were recorded on a Jobin-Yvon Horiba Fluorolog FL-3-11 Tau 3 spectrofluorimeter using band pathways of 3 nm for both excitation and emission. Phosphorescence lifetimes were recorded with a Fluoromax phosphorimeter accessory containing a UV xenon flash tube with a flash rate between 0.05 and 25 Hz. Phase shift and modulation were recorded over the frequency range of 0.1−100 MHz. Nanosecond lifetimes were recorded with an IBH 5000F coaxial nanosecond flashlamp. The lifetime data were fitted using the Jobin-Yvon software package and the Origin Pro 8 program. The quantum efficiency of the molecules in solution and the thin film configuration was determined using the quantum yield measurement system equipped with an integrated sphere from Hamamatsu model C9920-01.

The starting material $[Pt(bzq)(NCMe)_2]ClO_4$ was prepared as described elsewhere.[57] $C_7H_5NS_2$ and KOH were used as purchased from Aldrich and Panreac, respectively.

$KC_7H_4NS_2$. A solution of $C_7H_5NS_2$ (0.591 g, 3.532 mmol) in MeOH (5 mL) was added to a solution of KOH (0.198 g, 3.532 mmol) in MeOH (10 mL). The resulting yellow solution was stirred for 30 min, and then the solvent was evaporated to dryness. The residue was treated with ^{i}PrOH (2 mL), and the resulting yellow solid was filtered and dried. Yield: 0.546 g, 75%. Anal. Calcd for $KC_7H_4NS_2$: C, 40.94; H, 1.96; N, 6.82. Found: C, 40.65; H, 1.98; N, 7.12. ^1H NMR (acetone-d^6, 400.15 MHz, 298 K): δ 7.37 (1H, d, $J_{4'-5'}$ 7.8, $H^{4'}$), 7.25 (1H, d, $J_{7'-6'}$ 7.8, $H^{7'}$), 7.04 (1H, dd, $J_{6'-5'} = J_{6'-7'}$ 7.8, $H^{6'}$), 6.89 (2H, dd, $J_{5'-4'} = J_{5'-6'}$ 7.8, $H^{5'}$). IR (cm^{-1}): 1450 m, 1392 vs, 1377 vs, 1306 m, 1223 m, 1074 m, 1017 m, 998 s, 985 s, 934 m, 757 s, 748 vs, 724 vs, 656 m, 599 m, 440 m, 389 s, 379 s, 247 vs.

$[\{Pt(bzq)(C_7H_4NS_2)\}_2]\cdot Me_2CO$ (1). A solution of $KC_7H_4NS_2$ (0.095 g, 0.458 mmol) in MeOH (10 mL) was added to a yellow-orange suspension of $[Pt(bzq)(NCMe)_2]ClO_4$ (0.254 g, 0.458 mmol) in acetone (20 mL), and the reaction mixture was stirred for 2 h (see Scheme 1). The resulting orange-red precipitate was filtered and the solid was stirred in a mixture of acetone/MeOH (10/10 mL) for 45 min. Then, the solid was filtered and washed with MeOH (1 × 2 mL), Et_2O (2 × 2 mL) and dried yielding **1** (0.202 g, 78%). Anal. Calcd for $Pt_2C_{40}H_{24}N_4S_4\cdot Me_2CO$: C, 42.24; H, 2.66; N, 4.93. Found: C, 42.20; H, 2.27; N, 4.85. ^1H NMR (CD_2Cl_2, 400.16 MHz, 298K): δ 8.50−8.45 (2H, m, $H^{4'}$), 7.71 (2H, dd, J_{2-4} 0.9, J_{3-4} 8.0, H^4), 7.69−7.58 (6H, m, H^2, $H^{7'}$, H^9), 7.29−7.21 (6H, m, H^5, $H^{5'}$, $H^{6'}$), 7.07 (2H, AB, J_{5-6} 8.7, H^6), 7.06 (2H, d, J_{7-8} 7.4, H^7), 6.93 (2H, dd, J_{8-9} 7.4, H^8), 7.80 (2H, dd, J_{2-3} 5.3, H^3), 2.12 (6H, s, $(CH_3)_2CO$); ^{195}Pt NMR (CD_2Cl_2, 86.3 MHz, 298K): δ −3606.05. IR (cm^{-1}): ν(C═O) 1704 m, 1447 m, 1388 vs, 1326 m, 1247 m, 1082 m, 1026 s, 1009 s, 827 s, 818 s, 766 m, 751 vs, 723 m, 710 vs; ν(Pt−S) 400 s.

$[\{Pt(bzq)(C_7H_4NS_2)Cl\}_2]$ (2). A solution of Cl_2 in CCl_4 0.25 M (1.1 mL, 0.275 mmol) was added to an orange suspension of **1** (0.266 g, 0.234 mmol) in CH_2Cl_2 (5 mL) and the resulting red solution was stirred for 45 min, while a yellow-brown solid was precipitated. Then, Et_2O (10 mL) was added to the reaction mixture and the solid was filtered, washed with Et_2O (2 × 2 mL) and dried to the air, yielding complex **2** (0.233 g, 86%). Anal. Calcd for $Pt_2C_{40}H_{24}N_4S_4Cl_2\cdot 0.5CH_2Cl_2$: C, 40.79; H, 2.11; N, 4.70. Found: C, 40.70; H, 2.19; N, 4.62. ^1H NMR (CD_2Cl_2, 300.13 MHz, 193 K): δ 8.42 (2H, d, $J_{4'-5'}$ 8.1, $H^{4'}$), 7.85 (2H, d, $J_{7'-6'}$ 7.9, $H^{7'}$), 7.60 (2H, d, J_{4-3} 7.8, H^4), 7.47 (2H, dd, J_{9-7} 1.4, J_{9-8} 6.6, H^9), 7.42−7.27 (10H, m, H^2, H^5, H^8, H^7, $H^{6'}$), 7.22 (2H, dd, $J_{5'-4'}$ 7.9, $J_{5'-6'}$ 7.9 $H^{5'}$), 7.16 (2H, AB, J_{6-5} 8.8, H^6), 6.57 (2H, dd, J_{3-2} 5.5, H^3). IR (cm^{-1}): 1572 m, 1450 m, 1409 m, 1392 s, 1326 m, 1229 m, 1086 m, 1034 s, 1018 s, 928 m, 828 s, 818 m, 753 vs, 722 m, 710 vs, 512 m; ν(Pt−S) 436 s.

$[\{Pt(bzq)(C_7H_4NS_2)Br\}_2]$ (3). **3** was prepared in the same way as **2**, starting from Br_2 (solution in CH_2Cl_2, 0.25 M, 0.6 mL, 0.150 mmol); **1** (0.151 g, 0.133 mmol). Yield: (0.139 g, 85%). Anal. Calcd for $Pt_2C_{40}H_{24}N_4S_4Br_2\cdot CH_2Cl_2$: C, 37.20; H, 1.98; N, 4.23. Found: C, 37.13; H, 1.96; N, 4.21. ^1H NMR (CD_2Cl_2, 300.13 MHz, 193 K): δ 8.40 (2H, d, $J_{4'-5'}$ 8.4, $H^{4'}$), 7.84 (2H, d, $J_{7'-6'}$ 7.6, $H^{7'}$), 7.60 (2H, d, J_{4-3} 8.3, H^4), 7.46−7.25 (12H, m, H^2, H^5, H^8, H^7, H^9, $H^{6'}$), 7.24−7.13 (4H, m, $H^{5'}$, H^6), 6.57 (2H, dd, J_{3-2} 5.3, H^3). IR (cm^{-1}): 1573 m, 1450 m, 1409 m, 1391 s, 1326 m, 1227 m, 1139 m, 1110 m, 1085 s, 1033 vs, 1018 vs, 928 m, 827 vs, 818 m, 752 vs, 722 m, 709 vs, 511 m; ν(Pt−S) 436 s.

$[\{Pt(bzq)(C_7H_4NS_2)I\}_2]$ (4). A solution of I_2 (0.063 g, 0.248 mmol) in CH_2Cl_2 (13 mL) was added drop by drop to an orange suspension of **1** (0.159 g, 0.140 mmol) in CH_2Cl_2 (5 mL), and the resulting garnet-red solution was stirred for 75 min, while a violet solid was precipitated. The solvent was evaporated to ∼5 mL and Et_2O (10 mL) was added. The solid was filtered-off, washed with Et_2O (4 × 5 mL), and dried, yielding **4** (0.167 g, 89%). Anal. Calcd for $Pt_2C_{40}H_{24}N_4S_4I_2\cdot 3\,CH_2Cl_2$: C, 32.53; H, 1.90; N, 3.53. Found: C, 32.38; H, 1.66; N, 3.80. ^1H NMR (CD_2Cl_2, 300.13 MHz, 193 K): δ 8.31 (2H, d, $J_{4'-5'}$ 8.5, $H^{4'}$), 7.87 (2H, d, $J_{7'-6'}$ 7.8, $H^{7'}$), 7.65 (2H, d, J_{4-3} 8.4, H^4), 7.45−7.19 (16H, m, H^2, H^5, H^6, H^7, H^8, H^9, $H^{5'}$, $H^{6'}$), 6.62 (2H, dd, J_{3-2} 6.0, H^3). IR (cm^{-1}): 1571 m, 1449 m, 1407 m, 1392 s, 1325 m, 1228 m, 1138 m, 1109 m, 1084 s, 1030 vs, 1018 vs, 928 m, 827 vs, 817 m, 752 vs, 731 m, 709 vs, 509 s; ν(Pt−S) 438 m.

Scheme 1. Reactions and Numerical Scheme for ^1H NMR Purpose of 1−4

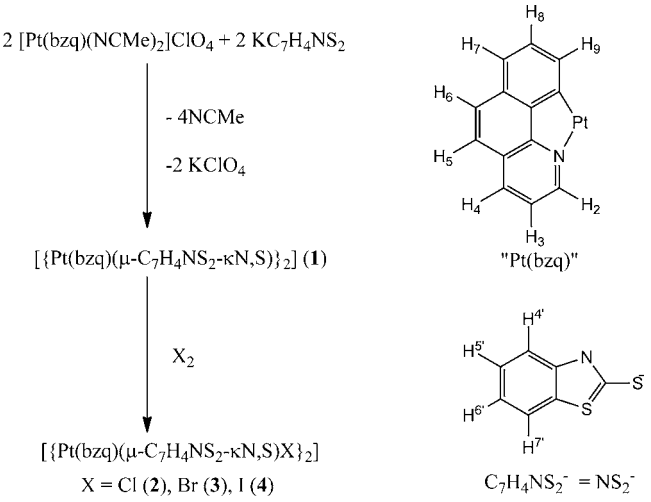

X-ray Structure Determinations. Crystal data and other details of the structure analyses are presented in Table 4. Suitable crystals for X-ray diffraction studies were obtained by slow diffusion of diethyl ether (**1**) or *n*-hexane (**2**−**4**) into concentrated solutions of the complexes in CH_2Cl_2. Crystals were mounted at the end of a quartz fiber. The radiation used in all cases was graphite monochromated $Mo_{K\alpha}$ (λ = 0.71 073 Å). X-ray intensity data were collected on an Oxford Diffraction Xcalibur diffractometer. The diffraction frames were integrated and corrected for absorption by using the CrysAlis RED program.[61] The structures were solved by Patterson and Fourier methods and refined by full-matrix least-squares on F^2 with SHELXL-97.[62] All non-hydrogen atoms were assigned anisotropic displacement parameters and refined without positional constraints, except as noted

dx.doi.org/10.1021/ic201910t | Inorg. Chem. 2012, 51, 3427−3435

Table 4. Crystal Data and Structure Refinement for Complexes $[\{Pt(bzq)(C_7H_4NS_2)\}_2]\cdot Me_2CO$ (**1**·Me_2CO), $[\{Pt(bzq)(C_7H_4NS_2)Cl\}_2]\cdot 2.5CH_2Cl_2$ (**2**·$2.5CH_2Cl_2$), $[\{Pt(bzq)(C_7H_4NS_2)Br\}_2]\cdot 3CH_2Cl_2$ (**3**·$3CH_2Cl_2$), and $[\{Pt(bzq)(C_7H_4NS_2)I\}_2]\cdot 3CH_2Cl_2$ (**4**·$3CH_2Cl_2$)

	1·Me_2CO	**2**·$2.5CH_2Cl_2$	**3**·$3CH_2Cl_2$	**4**·$3CH_2Cl_2$
formula	$C_{40}H_{24}N_4Pt_2S_4\cdot Me_2CO$	$C_{40}H_{24}Cl_2N_4Pt_2S_4\cdot 2.5CH_2Cl_2$	$C_{40}H_{24}Br_2N_4Pt_2S_4\cdot 3CH_2Cl_2$	$C_{40}H_{24}I_2N_4Pt_2S_4\cdot 3CH_2Cl_2$
M_t [g mol^{-1}]	1137.13	1362.27	1493.65	1587.63
T [K]	100(1)	100(1)	100(1)	100(1)
λ [Å]	0.710 73	0.710 73	0.710 73	0.710 73
crystal system	triclinic	triclinic	monoclinic	monoclinic
space group	$P\bar{1}$	$P\bar{1}$	$P2_1/n$	$P2_1/n$
a [Å]	11.1819(3)	13.3386(2)	17.1442(3)	17.3898(2)
b [Å]	11.7099(3)	17.2028(3)	14.5836(2)	14.9110(1)
c [Å]	15.5443(4)	19.0478(3)	20.0940(4)	20.1614(3)
α [deg]	84.613(2)	91.242(1)	90	90
β [deg]	73.393(2)	95.097(1)	112.661(2)	113.379(2)
γ [deg]	71.687(2)	98.189(1)	90	90
V [Å^3]	1851.65(8)	4306.45(12)	4636.13(14)	4798.63(10)
Z	2	4	4	4
ρ [g cm^{-3}]	2.040	2.101	2.140	2.198
μ [mm^{-1}]	7.815	7.158	8.316	7.656
$F(000)$	1088	2604	2832	2976
2θ range [deg]	7.6−57.8	8.4−57.9	8.2−57.7	8.2−57.7
no. of reflns collected	27557	92989	51290	52416
no. of unique reflns	8308	20608	11062	11440
R(int)	0.0277	0.0482	0.0434	0.0354
final R indices [$I > 2\theta(I)$][a]				
R_1	0.0202	0.0369	0.0406	0.0383
wR_2	0.0413	0.0898	0.1064	0.0917
R indices (all data)				
R_1	0.0277	0.0533	0.0533	0.0439
wR_2	0.0424	0.0932	0.1103	0.0935
goodness-of-fit on F^2[b]	1.022	1.007	1.076	1.045

[a] $R_1 = \sum(||F_o| - |F_c||)/\sum|F_o|$. $wR_2 = [\sum w(F_o^2 - F_c^2)^2/\sum w(F_o^2)^2]^{1/2}$. [b] Goodness-of-fit $= [\sum w(F_o^2 - F_c^2)^2/(n_{obs} - n_{param})]^{1/2}$.

below. All hydrogen atoms were constrained to idealized geometries and assigned isotropic displacement parameters equal to 1.2 times the U_{iso} values of their attached parent atoms (1.5 times for the methyl hydrogen atoms). In the structure of **3**·$3CH_2Cl_2$, the dichloromethane solvent molecules were very diffuse and restraints in their geometry and thermal parameters were used. Full-matrix least-squares refinement of these models against F^2 converged to the final residual indices given in Table 4.

Computational Details. The computational method used was density functional theory (DFT) with the M06 hybrid functional,[63] using the Gaussian 09[64] program package. The basis set used was the LanL2TZ(f) effective core potential for the platinum atoms and 6-311G(d,p) for the remaining atoms. Geometry optimizations were performed in the presence of dichloromethane with the polarizable continuum model (PCM), using the integral equation formalism variant (IEFPCM). TD-DFT calculations were also carried out using the same solvation model, as implemented in the Gaussian 09 software.

■ ASSOCIATED CONTENT

Supporting Information

Molecular and supramolecular structures of compounds **3** and **4**; UV−vis absorption spectra of **1** and the ligand NS_2H in CH_2Cl_2 (10^{-3} M) at room temperature; low-energy region of the UV−vis spectra of **1** in CH_2Cl_2 (298 K) at different concentrations and representation of the linear fit of the absorbance at 487 nm (A_{487}) vs concentration; normalized excitation and emission spectra of **1** in 2-Me-THF (10^{-4} M) at 298 and 77 K; TGA of **1** under Ar at 1 atm; DFT-optimized structure and optimized coordinates of complex $[\{Pt(bzq)(\mu\text{-}C_7H_4NS_2\text{-}\kappa N,S)\}_2]$; representative frontier orbitals for $[\{Pt(bzq)(\mu\text{-}C_7H_4NS_2\text{-}\kappa N,S)\}_2]$; composition of frontier MOs in the ground state for **1** in CH_2Cl_2 solution; TD-DFT excitation calculations for **1** in CH_2Cl_2; DFT-optimized coordinates of $[\{Pt(bzq)(\mu\text{-}C_7H_4NS_2\text{-}\kappa N,S)\}_2]$ in the excited stated, T_1. This material is available free of charge via the Internet at http://pubs.acs.org.

■ AUTHOR INFORMATION

Corresponding Author

*E-mail: sicilia@unizar.es.

Notes

The authors declare no competing financial interest.

■ ACKNOWLEDGMENTS

This work was supported by the Spanish MICINN/FEDER (Project CTQ2008-06669-C02), MICINN/FEDER (Project CTQ2008-03860), and the Gobierno de Aragón (Grupo Consolidado: Química Inorgánica y de los Compuestos Organometálicos). D.T. and P. B. acknowledge the support of a FPU and FPI grants, respectively, from the MICINN.

■ REFERENCES

(1) Kato, M. *Bull. Chem. Soc. Jpn.* **2007**, *80*, 287.
(2) Williams, J. A. G. *Top. Curr. Chem.* **2007**, *281*, 205.
(3) Williams, J. A. G.; Develay, S.; Rochester, D. L.; Murphy, L. *Coord. Chem. Rev.* **2008**, *252*, 2596.
(4) Williams, J. A. G. *Chem. Soc. Rev.* **2009**, *38*, 1783.

(5) Murphy, L.; Williams, J. A. G. *Top. Organomet. Chem.* **2010**, *28*, 75.
(6) Williams, J. A. G. Molecular Organometallic Materials for Optics. In *Topics in Organometallic Chemistry*; Bozec, H., Guerchais, V., Eds.; Springer: New York, 2009.
(7) Xiang, H. F.; Lai, S. W.; Lai, P. T.; Che, C. M. Phosphorescent platinum(II) materials for OLED applications. In *Highly Efficient OLEDs with Phosphorescent Materials*; Yersin, H., Ed.; Wiley-VCH: Weinheim, Germany, 2007.
(8) Yang, C.; Zhang, X.; You, H.; Zhu, L.; Chen, L.; Zhu, L.; Tao, Y.; Ma, D.; Shuai, Z.; Qin, J. *Adv. Funct. Mater.* **2007**, *17*, 651.
(9) Connick, W. B.; Henling, L. M.; Marsh, R. E.; Gray, H. B. *Inorg. Chem.* **1996**, *35*, 6261.
(10) Connick, W. B.; Henling, L. M.; Marsh, R. E. *Acta Crystallogr., Sect. B* **1996**, *52*, 817.
(11) Connick, W. B.; Marsh, R. E.; Schaefer, W. P.; Gray, H. B. *Inorg. Chem.* **1997**, *36*, 913.
(12) Kato, M.; Kosuge, C.; Morii, K.; Ahn, J. S.; Kitagawa, H.; Mitani, T.; Matsushita, M.; Kato, T.; Yano, S.; Kimura, M. *Inorg. Chem.* **1999**, *38*, 1638.
(13) Buss, C. E.; Mann, K. R. *J. Am. Chem. Soc.* **2002**, *124*, 1031−1039.
(14) Dylla, A. G.; Janzen, D. E.; Pomije, M. K.; Mann, K. R. *Organometallics* **2007**, *26*, 6243.
(15) Sun, Y.; Ye, K.; Zhang, H.; Zhang, J.; Zhao, L.; Li, B.; Yang, G.; Yang, B.; Wang, Y.; Lai, S. W.; Che, C. M. *Angew. Chem., Int. Ed.* **2006**, *45*, 5610.
(16) Díez, A.; Fornies, J.; Larraz, C.; Lalinde, E.; López, J. A.; Martin, A.; Moreno, M. T.; Sicilia, V. *Inorg. Chem.* **2010**, *49*, 3239.
(17) Holland, L.; Shen, W.-Z.; von Grebe, P.; Sanz Miguel, P. J.; Pichierri, F.; Springer, A.; Schalley, C. A.; Lippert, B. *Dalton Trans.* **2011**, *40*, 5159.
(18) Eryazici, I.; Moorefield, C. N.; Newkome, G. R. *Chem. Rev.* **2008**, *108*, 1834.
(19) Moussa, J.; Wong, K. M. C.; Chamoreau, L. M.; Amouri, H.; Yam, V. W. W. *Dalton Trans.* **2007**, 3526.
(20) Wong, K. M. C.; Yam, V. W. W. *Acc. Chem. Res.* **2011**, *44*, 424.
(21) Lu, W.; Mi, B. X.; Chan, M. C. W.; Hui, Z.; Che, C. M.; Zhu, N. L., S. T. *J. Am. Chem. Soc.* **2004**, *126*, 4958.
(22) Anderson, B. M.; Hurst, S. K. *Eur. J. Inorg. Chem.* **2009**, *21*, 3041.
(23) Kui, S. C. F.; Chui, S. S. Y.; Che, C. M.; Zhu, N. *J. Am. Chem. Soc.* **2006**, *128*, 8297.
(24) Yam, V. W. W.; Chan, K. H. Y.; Wong, K. M. C.; Zhu, N. *Chem.—Eur. J.* **2005**, *11*, 4535.
(25) Utsono, M.; Yutaka, T.; Murata, M.; Kurihara, M.; Tamai, N.; Nishihara, H. *Inorg. Chem.* **2007**, *46*, 11291.
(26) Poater, A.; Moradell, S.; Pinilla, E.; Poater, J.; Solá, M.; Martínez, M. A.; Llobet, A. *Dalton Trans.* **2006**, 1188.
(27) Ding, J.; Pan, D.; Tung, C. H.; Wu, L. Z. *Inorg. Chem.* **2008**, *47*, 5099.
(28) Lai, S. W.; Lam, H. W.; Lu, W.; Cheung, K. K.; Che, C. M. *Organometallics* **2001**, *21*, 226.
(29) Lu, W.; Chan, M. C. W.; Zhu, N.; Che, C. M.; Li, C.; Hui, Z. *J. Am. Chem. Soc.* **2004**, *126*, 7639.
(30) Díez, A.; Forniés, J.; Fuertes, S.; Larraz, C.; Lalinde, E.; López, J. A.; Martín, A.; Moreno, M. T.; Sicilia, V. *Organometallics* **2009**, *28*, 1705.
(31) Tam, A. Y. Y.; Wong, K. M. C.; Wang, G.; Yam, V. W. W. *Chem. Commun.* **2007**, 2028.
(32) Yam, V. W. W.; Wong, K. M. C.; Zhu, N. *J. Am. Chem. Soc.* **2002**, *124*, 6506.
(33) Che, C. M.; He, L. Y.; Poon, C. K.; Mak, T. C. W. *Inorg. Chem.* **1989**, *28*, 3081.
(34) Bennett, M. A.; Bhargava, S. K.; Cheng, E. C. C.; Lam, W. H.; Lee, T. K. M.; Privér, S. H.; Wagler, J.; Willis, A. C.; Yam, V. W. W. *J. Am. Chem. Soc.* **2010**, *132*, 7094.
(35) Aoki, R.; Kobayashi, A.; Chang, H.; Kato, M. *Bull. Chem. Soc. Jpn.* **2011**, *84*, 218.
(36) Che, C. M.; Herbstein, F. H.; Schaefer, W. P.; Marsh, R. E.; Gray, H. B. *J. Am. Chem. Soc.* **1983**, *105*, 4604.
(37) Marsh, R. E.; Herbstein, F. H. *Acta Crystallogr., Sect.B: Struct. Sci.* **1983**, *B39*, 280.
(38) Marino, N.; Fazen, C.; Blakemore, J.; Incarvito, C. D.; Hazari, N.; Doyle, R. P. *Inorg. Chem.* **2011**, *50*, 2507.
(39) Umakoshi, K.; Kinoshita, I.; Ichamura, A.; Ooi, S. *Inorg. Chem.* **1987**, *26*, 3551.
(40) Kato, M.; Omura, A.; Toshikawa, A.; Kishi, S.; Sugimoto, Y. *Angew. Chem., Int. Ed.* **2002**, *41*, 3183.
(41) Tzeng, B.; Fu, W.; Che, C.; Chao, H.; Cheung, K.; Peng, S. *J. Chem. Soc., Dalton Trans.* **1999**, 1017.
(42) Liu, F.; Chen, W.; Wang, D. *Dalton Trans.* **2006**, 3445.
(43) Chen, W.; Matsumoto, K. *Inorg. Chim. Acta* **2003**, *342*, 88.
(44) Yam, V. W.; Yu, K.; Wong, K. M.; Cheung, K. *Organometallics* **2001**, *20*, 721.
(45) Tzeng, B. C.; Chiu, T. H.; Lin, S. Y.; Yang, C. M.; Chang, T. Y.; Huang, C. H.; Chang, A. H. H.; Lee, G. H. *Cryst. Growth Des.* **2009**, *9*, 5356.
(46) Roundhill, D. M.; Gray, H. B.; Che, C. M. *Acc. Chem. Res.* **1989**, *22*, 55.
(47) Alexander, K. A.; Bryan, S. A.; Fronczek, F. R.; Fultz, W. C.; Rheingold, A. L.; Roundhill, D. M.; Stein, P.; Watkins, S. F. *Inorg. Chem.* **1985**, *24*, 2803.
(48) Che, C. M.; Schaefer, W. P.; Gray, H. B.; Dickson, M. K.; Stein, P. B.; Roundhill, D. M. *J. Am. Chem. Soc.* **1982**, *104*, 4253.
(49) Koshiyama, T.; Kato, M. *Acta Crystallogr.* **2005**, *C61*, m173.
(50) Stiegman, A. E.; Miskovski, V. M.; Gray, H. B. *J. Am. Chem. Soc.* **1986**, *108*, 2781.
(51) Bellito, C.; Flamini, A.; Piovesana, O.; Zanazzi, P. F. *Inorg. Chem.* **1980**, *19*, 3632.
(52) Kishi, S.; Kato, M. *Mol. Cryst. Liq. Cryst.* **2002**, *379*, 303.
(53) Díez, A.; Fornies, J.; García, A.; Lalinde, E.; Moreno, M. T. *Inorg. Chem.* **2005**, *44*, 2443.
(54) Fernández, S.; Fornies, J.; Gil, B.; Gómez, J.; Lalinde, E. *Dalton Trans.* **2003**, 822.
(55) Flemming, J. P.; Pilon, M. C.; Borbulevitch, O. Y.; Antipin, M. Y.; Grushin, V. V. *Inorg. Chim. Acta* **1998**, *280*, 87.
(56) Bennett, M. A.; Bhargava, S. K.; Bond, A. M.; Edwards, A. J.; Guo, S.-X.; Privér, S. H.; Rae, A. D.; Willis, A. C. *Inorg. Chem.* **2004**, *43*, 7752.
(57) Forniés, J.; Fuertes, S.; López, J. A.; Martín, A.; Sicilia, V. *Inorg. Chem.* **2008**, *47*, 7166.
(58) Vezzu, D. A. K.; Deaton, J. C.; Jones, J. S.; Bartolotti, L.; Harris, C. F.; Marchetti, A. P.; Kondakova, M.; Pike, R. D.; Huo, S. *Inorg. Chem.* **2010**, *49*, 5107.
(59) Nazeeruddin, M. K.; Grätzel, M. *Struct. Bonding (Berlin, Ger.)* **2007**, *123*, 113.
(60) Aullón, G.; Álvarez, S. *Chem.—Eur. J.* **1997**, *3*, 655.
(61) *CrysAlis RED, Program for X-ray CCD camera data reduction*, version 1.171.32.19; Oxford Diffraction Ltd., Oxford, United Kingdom, 2008.
(62) Sheldrick, G. M. *SHELXL-97, A Program for Crystal Structure Determination*. University of Göttingen: Göttingen, Germany, 1997.
(63) Zhao, Y.; Truhlar, D. G. *Theor. Chem. Acc.* **2008**, *120*, 215.
(64) Frisch, M. J.; Trucks, G. W.; Schlegel, H. B.; Scuseria, G. E.; Robb, M. A.; Cheeseman, J. R.; Scalmani, G.; Barone, V.; Mennucci, B.; Petersson, G. A.; Nakatsuji, H.; Caricato, M.; Li, X.; Hratchian, H. P.; Izmaylov, A. F.; Bloino, J.; Zheng, G.; Sonnenberg, J. L.; Hada, M.; Ehara, M.; Toyota, K.; Fukuda, R.; Hasegawa, J.; Ishida, M.; Nakajima, T.; Honda, Y.; Kitao, O.; Nakai, H.; Vreven, T.; Montgomery, J. A., Jr. ; Peralta, J. E.; Ogliaro, F.; Bearpark, M.; Heyd, J. J.; Brothers, E.; Kudin, K. N.; Staroverov, V. N.; Kobayashi, R.; Normand, J.; Raghavachari, K.; Rendell, A.; Burant, J. C.; Iyengar, S. S.; Tomasi, J.; Cossi, M.; Rega, N.; Millam, N. J.; Klene, M.; Knox, J. E.; Cross, J. B.; Bakken, V.; Adamo, C.; Jaramillo, J.; Gomperts, R.; Stratmann, R. E.; Yazyev, O.; Austin, A. J.; Cammi, R.; Pomelli, C.; Ochterski, J. W.; Martin, R. L.; Morokuma, K.; Zakrzewski, V. G.; Voth, G. A.; Salvador, P.; Dannenberg, J. J.; Dapprich, S.; Daniels, A. D.; Farkas, O.; Foresman, J. B.; Ortiz, J. V.; Cioslowski, J.; Fox, D. J. *Gaussian 09*, revision A.02; Gaussian, Inc.: Wallingford, CT, 2009.